Supporting Information

Roebroeks et al. 10.1073/pnas.1112261109

SI Text

Physical Properties Study. ***Methods.*** To study the physical properties of the possible hematite concentrates from the Maastricht-Belvédère excavations, we analyzed three samples (Cz11-1, WW10-8, and 20/23–1) by environmental scanning electron microscopy (ESEM), energy-dispersive X-ray spectroscopy (EDX), X-ray diffraction (XRD), and rockmagnetic measurements. Samples were analyzed at the Geochronology Laboratory of the Centro Nacional de Investigación Sobre la Evolución Humana, Burgos, Spain. In addition, samples Bz13-6 and Dz20-56 (from site C) were submitted to thin section analysis at the same laboratory.

ESEM and EDX. Samples were photographed using a Fei Quanta 600 ESEM system, and microanalyses were performed with an Oxford INCA 350 EDX spectroscopy microanalysis system. EDX is a nondestructive analytical technique used for elemental analysis or chemical characterization of samples, which measures the energy of the scattered X-rays when an electron beam impacts on a sample. The ESEM photographs were used to evaluate the samples and their relationship with the surrounding matrix, if present. Observations were made both before and after samples were cut with a diamond hair cutter to get a smooth surface.

XRD. The mineralogic composition of the samples was analyzed by XRD. Patterns were collected with a Panalytical XPert PRO MPD diffractometer with CuKα radiation (λ = 1.5406 Å) and a solid-state multichannel detector. Samples were analyzed as bulk powder samples with a reflection-transmission spinner stage and as solid samples by placing specimens on a multipurpose sample stage. The following analysis parameters were used: 45 kV, beam current of 40 mA, scan range of 5°–70° 2θ in continuous scan of 0.02° 2θ steps, with 100–700 s per step. The diffraction patterns were compared with the International Centre for Diffraction Data database using XPert High Score Plus software.

Rockmagnetism. A vibrating sample magnetometer (MicroMag Model 3900; Princeton Measurements), was used to measure hysteresis loops, single moment-vs.-temperature curves, and acquisition curves of isothermal remanent magnetization (IRM). Measurements were obtained at room temperature and single moment-vs.-temperature measurements within the range of room temperature and to a maximum of 750 °C. Data acquired from the IRM measurements were imported in a specially developed Excel worksheet (1), which can be downloaded at http://www.geo.uu.nl/~forth/. The base function fitting of the IRM acquisition curves is based on a cumulative log Gaussian analysis developed by Robertson and France (2) and extended by Kruiver et al. (1). This method makes it possible to differentiate magnetic mineral phases from the IRM data.

Results

ESEM and EDX. Two of the three samples were retrieved situated in their sedimentary matrix. Two of these samples (Cz11-1, from site C and 20/23–1, from site F) had sharp boundaries with their matrix. Sample 20/23–1 had a separation from the matrix (Fig. S1, *Top*), which is not present in sample Cz11-1 (Fig. S2*A*). All EDX data show that the samples have an increased iron content, and for two samples with matrix, an increased iron content in relation to the matrix (Fig. S1, *Middle* and *Bottom*).

XRD. All XRD measurements for the three samples clearly identify several minerals, including quartz and hematite (Fig. S4). Sample 20/23–1 also contains clearly identifiable albite and goethite. Sample Cz11-1 contains rutile and an additional iron oxide with low crystallinity that could not be identified. Sample WW108 contains, along with the hematite and quartz, a second form of quartz, muscovite, and zircon. It is important to note that the quantification of the different minerals (Fig. S4) is meaningless, given that the beam of the XRD is larger than the size of the samples, resulting in underestimates of hematite. Our results confirm the previous analyses by Arps (3), who used a Guinier–de Wolf quadruple focusing camera (Enraf Nonius) for an XRD study of three of the hematite finds from Maastricht-Belvédère. His analysis indicated that the samples consisted of a mixture of quartz (the strongest signal) and hematite, which was considered responsible for the red stains in the silty fine-sand deposits at Maastricht-Belvédère.

Rockmagnetism. Sample Cz11-1 was of insufficient size for rock magnetic measurements. Samples 20/23–1 and WW10-8 yielded similar results, with the latter sample (from site C) providing the clearest data, due to sample size. The hysteresis curves show (Fig. S5) both paramagnetic and ferromagnetic contributions and saturation not is reached at 1.3 T, revealing the presence of a high-coercivity magnetic phase.

The IRM acquisition curves (Fig. S3) are in agreement with the hysteresis curves, in that a high-coercivity component is the main magnetic component in these samples. IRM line-fitting using the Kruiver et al. (1) method actually reveals two magnetic components. Component 1 is an artifact (4, 5) and is not discussed further. The artifact is a result of the log Gaussian base function method of fitting, which can fit only distributions that are symmetric in the log-field space. Left-skewed distributions (a consequence of time-dependent magnetic behavior and/or magnetic interaction) must be fitted in the package of Kruiver et al. (1) with an extra component with log B1/2 of ∼1.0. The amount (SIRM value) of the skewed artifact component has to be added to the SIRM of the dominant coercivity component (with log B1/2 of 1.4–1.8) to give the true intensity of this dominant component. Components 2 and 3, with log B1/2 values of 2.45, DP 0.25 and 2.95, DP 0.29, respectively, receive physical interpretation.

The magnetic moment-vs.-temperature data of sample WW10-8 (Fig. S7) shows a slightly declining trend until 450 °C, after which the magnet moment increases to return to a pre-450 °C level at ∼650 °C.

Discussion

All of the data obtained by the different methods clearly indicate the presence of hematite in the three samples analyzed. EDX demonstrated an increased percentage of iron oxide in the samples in relation to their matrix, whereas XRD positively identified hematite as a compound in the sample. Unfortunately, the small size of the samples precludes the semiquantification of the mineral components.

The rockmagnetic data, like the XRD data, revealed hematite in all samples analyzed. The hysteresis curve and IRM showed a high-coercivity component generally interpreted as hematite or goethite. Line-fitting of the IRM data identified two components with high log B1/2 values. We consider the component with a log B1/2 of 2.45 to be hematite, whereas the second component, with a value of log B1/2 of ∼2.95, may be either hematite of different grain size or goethite. Goethite has a low Curie temperature of ∼120 °C. The single moment-vs.- temperature curve does not show a drop in magnetic moment at this temperature, suggesting that goethite is not present in sufficient amounts in the sample. Because of thermochemical reactions (see ref. 6) in the sample starting at 450 °C, most likely due to formation of magnetite, precluding further identification of magnetic minerals after this temperature.

Experimentally Produced Hematite Concentrates in the Site C Matrix. Microscopic examination of the hematite concentrates by one investigator (C.E.S.A.) revealed a red staining agent surrounding the quartz grains of the sedimentary matrix as a very thin coating, with occasional clots composed of the fine red material and the clay and silt particles of the sediment (3) (Fig. S8). Importantly, individual reddish crystal grains (e.g., hematite) were not visible. The boundary between the sedimentary matrix and the concentrates was sharp in thin sections as well (Fig. S9), with the hematite concentrate itself more fine-grained than the matrix. This finding seems to imply that the red material entered the sediments after their formation. We hypothesized that the red material was originally concentrated in a liquid solution/paste, and that blobs of this substance became embedded in the sediments during use of the liquefied substance, spilled on the soil surface. To test this interpretation, we performed a small experiment to observe the impact of drops of a "hematite liquid" on the site C sediment.

Air-dried, very-fine sand from the matrix of the site C finds (still available from sediment samples from excavation square Pz15) was packed in plastic Petri dishes (Fig. S10). The sediment was then submitted to droplets of a liquid consisting of a mix of hematite powder and rainwater (1 g of hematite in 20 mL of water), produced at 20 °C. The hematite powder was obtained by grinding a hematite nodule on a quartzitic sandstone Maas River pebble.

The drops, 0.3 mm in diameter, were produced with a 2.5-mL plastic pipette and launched manually from a height of 50 cm. The impact of the drops created well-delimited hematite dots in the dry sediment, all smaller than 1 cm (Fig. S10 *A* and *B*). Increasing the launch height to 150 cm led to somewhat larger dots, as did increasing the drop size from ∼0.3 to ∼0.5 cm (Fig. S10 *C* and *D*). In both cases, concentrates of ∼1 cm in diameter were produced. As the pictures show, the drops' impact pressure created both a compression pit and a compensatory bulge around the perimeter of the pit–a phenomenon well known from experimental studies of the impact of raindrops on sediments (7, 8). The red material was contained at the bottom of these impact craters. The resulting hematite concentrates consisted of small semicircular discs with a thickness of 1–2 mm, sometimes with a thin rim around their perimeter (the compensatory bulge mentioned above).

These experiments simulated the impact of drops under very dry conditions. To simulate more humid (and probably more realistic) conditions in a separate run, we poured 2 mL of rainwater into the Petri dish, then gently poured in the air-dried sediment. The sediment-filled Petri dish was then allowed to dry at room temperature for 24 h, resulting in more humid and more compacted sediment compared with that used in the previous experiments. The resulting depressions containing the hematite liquid lacked the characteristic rim usually produced in the dry sediments (Fig. S11). To simulate a larger spill of the liquid, we poured 2 mL of the 1:20 solution onto the sediment from a test tube held ∼5 cm above a sediment-filled disk. This created a well-delimited (2 cm in maximum dimension and ∼2 mm thick) hematite concentration in the sediment that is (Fig. S12).

Our experiments produced concentrates of hematite material with close similarities to the archeological finds (compare Figs. S8 and S11), both macroscopically and microscopically. The results with the humid sediments provided the strongest similarities, with less pronounced or absent characteristic rims around the perimeter. One difference between the experimental and the archeological specimens is the denser concentrations of the red material in the latter. This may be related to the smaller hematite powder-to-liquid ratio in the past (i.e., more hematite powder used than in the experiment) and to the fact that water was the only liquid used in the small experiment, leading to a more diluted solution in the matrix than had fatty substances been added/used as a "carrier" for the hematite powder. Apart from this obvious difference between the composition of the experimental liquid mixture and the (unknown) past liquid, there are more limitations on the value of this experiment. We have no idea about the humidity of the sediment matrix during creation of the archeological concentrates and only very indirect indications about the vegetation of the surface during hominin presence (certainly not as barren as in our experiment). After being created, the archeological specimens were covered by fine-grained fluvial sediments and subjected to various chemical and compaction processes during the 250,000 y that they spend in their matrix. Despite this, they were still sufficiently visible to be recovered during archeological excavation.

1. Kruiver PP, Dekkers MJ, Heslop D (2001) Quantification of magnetic coercivity components by the analysis of acquisition curves of isothermal remanent magnetisation. *Earth Planet Sci Lett* 189:269–276.
2. Robertson DJ, France DE (1994) Discrimination of remanence-carrying minerals in mixtures, using isothermal remanent magnetisation acquisition curves. *Phys Earth Planet Inter* 82:223–234.
3. Arps CES (1988) The identification of haematite as the colouring agent in red ochre from the Middle Palaeolithic site C at Maastricht-Belvédère, The Netherlands, by means of x-ray diffraction analysis. *Analecta Praehistorica Leidensia* 21:163–165.
4. Egli R (2004) Characterization of individual rock magnetic components by analysis of remanence curves, 3: Bacterial magnetite and natural processes in lakes. *Phys Chem Earth Parts ABC* 29:869–884.
5. Heslop D, McIntosh G, Dekkers MJ (2004) Using time- and temperature-dependent Preisach models to investigate the limitations of modelling isothermal remanent magnetization acquisition curves with cumulative log Gaussian functions. *Geophys J Int* 157:55–63.
6. Dekkers MJ (1988) Some rockmagnetic parameters for natural goethite, pyrrhotite and fine-grained hematite. PhD thesis (University of Utrecht, Utrecht, The Netherlands).
7. Huang C, Bradford JM, Cushman JM (1983) A numerical study of raindrop impact phenomena: The elastic deformation case. *J Soil Sci Soc Am* 47:855–861.
8. Terry JP (1998) A rainsplash component analysis to define mechanisms of soil detachment and transportation. *Aust J Soil Res* 36:525–542.

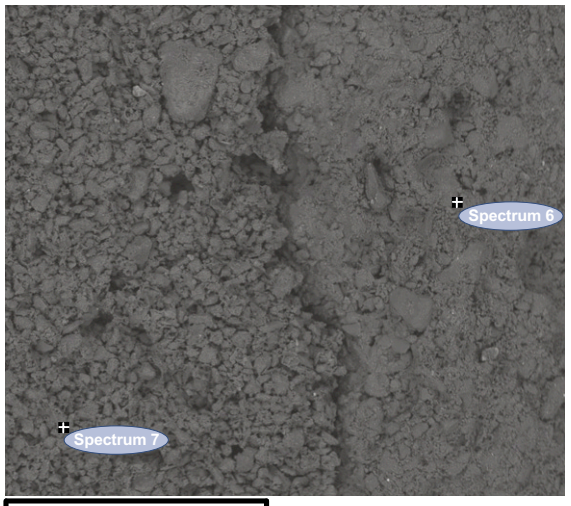

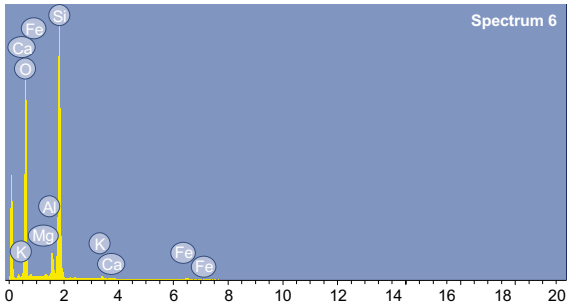

Elements	Weight%	Atomic%
O K	62.34	74.85
Mg K	0.21	0.16
Al K	2.36	1.68
Si K	32.75	22.40
K K	0.47	0.23
Ca K	0.26	0.13
Fe K	1.61	0.55
Totals	100.00	

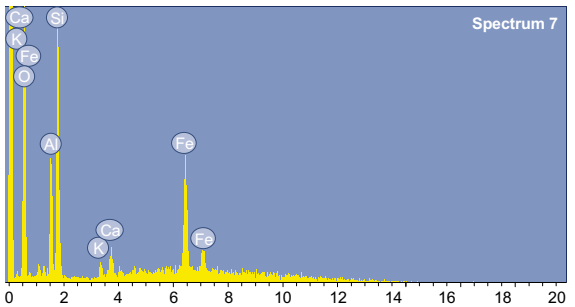

Elements	Weight%	Atomic%
O K	32.36	55.38
Al K	6.50	6.60
Si K	14.81	14.44
K K	1.47	1.03
Ca K	2.93	2.00
Fe K	41.91	20.55
Totals	100.00	

Fig. S1. (*Top*) ESEM image of sample 20/23–1 (site F) (*Left*) and the sediment matrix (*Right*). (*Middle*) Mineralogic composition of the sediment matrix. (*Bottom*) Mineralogic composition of sample 20/23–1.

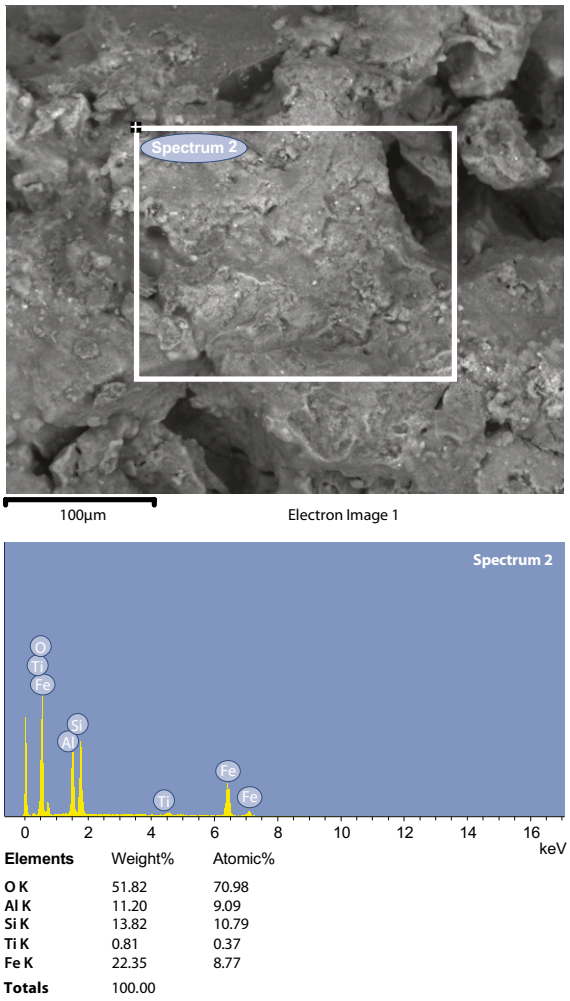

Elements	Weight%	Atomic%
O K	51.82	70.98
Al K	11.20	9.09
Si K	13.82	10.79
Ti K	0.81	0.37
Fe K	22.35	8.77
Totals	100.00	

Fig. S2. (*Upper*) ESEM image of sample Cz11-1 (site C). (*Lower*) Mineralogic composition of sample Cz11-1.

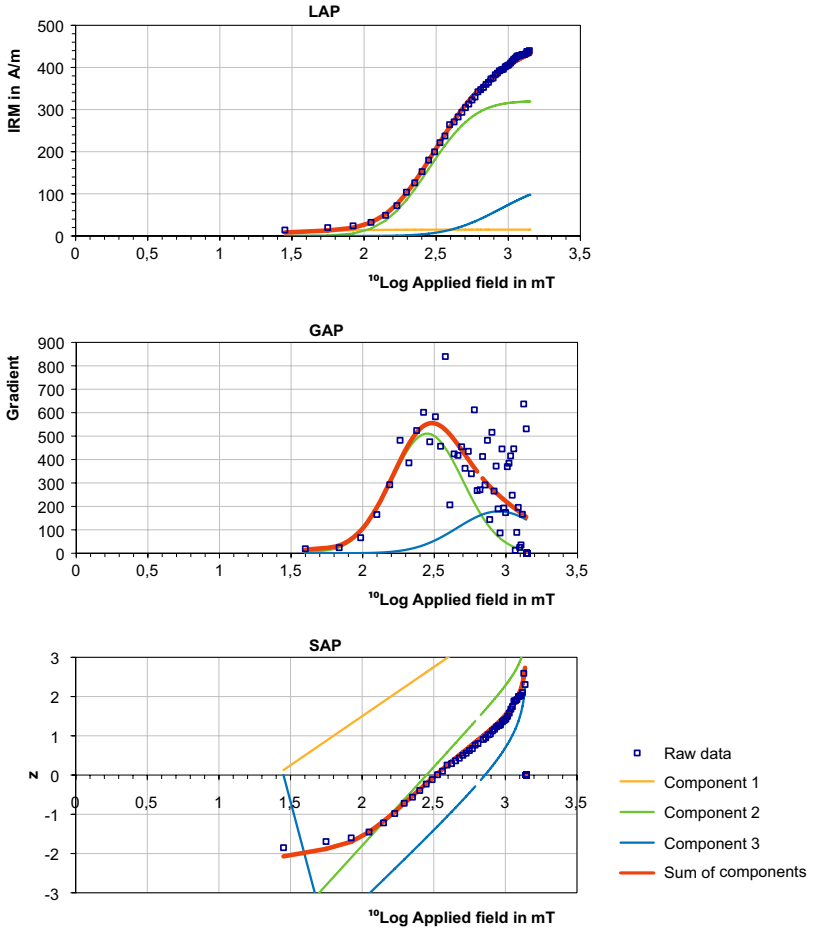

Fig. S3. IRM component analyses of sample WW10-8 (site C).

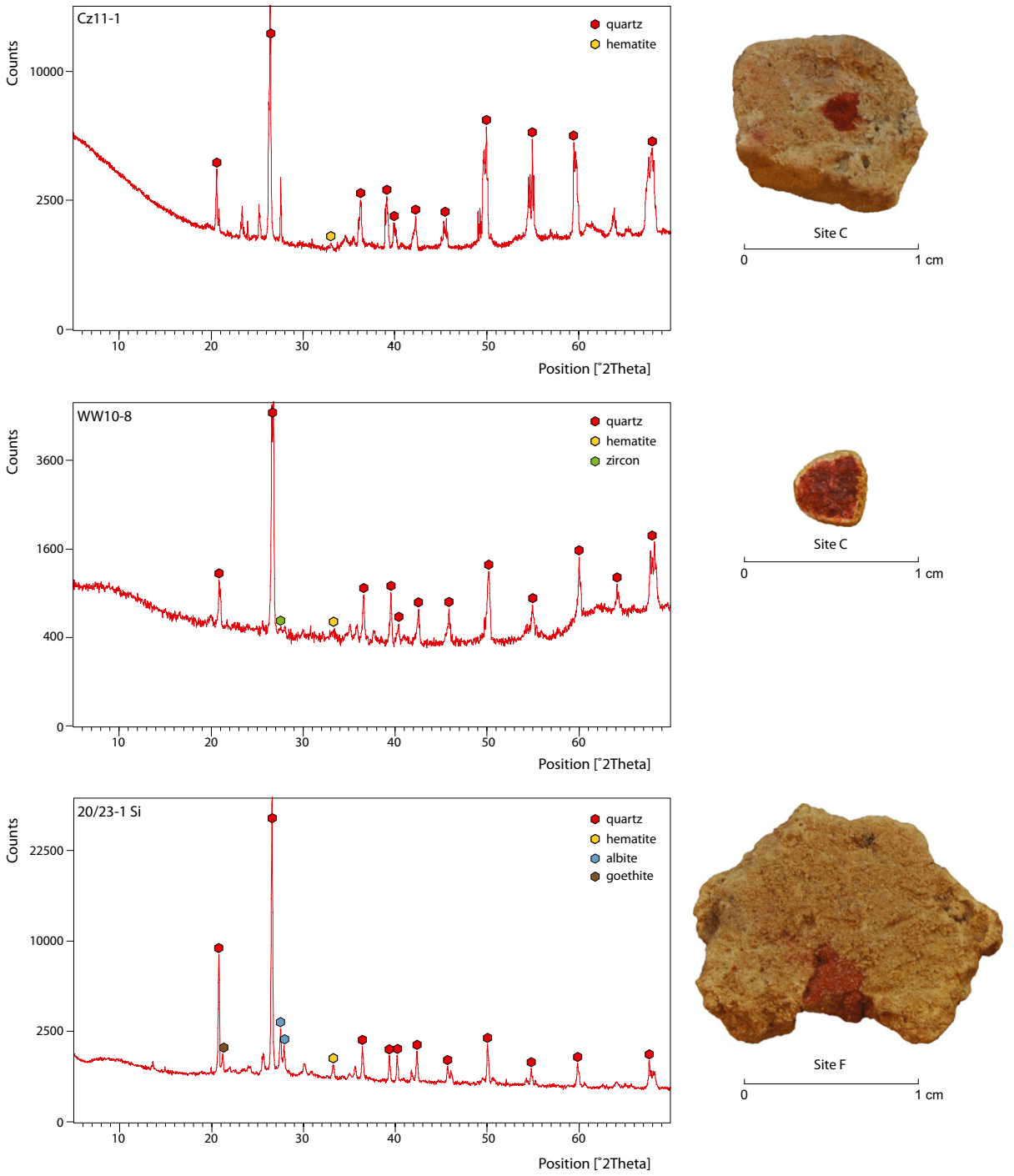

Fig. S4. XRD analyses of samples Cz11-1 (site C) (*Top*), WW10-8 (site C) (*Middle*), and 20–23/1 (site F) (*Bottom*).

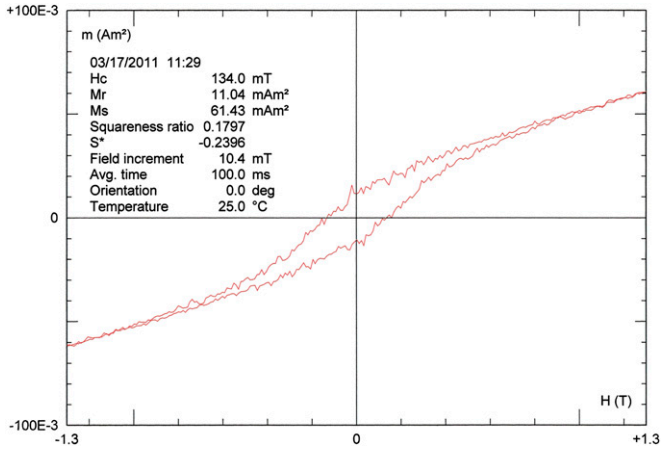

Fig. S5. Hysteresis, uncorrected for slope, curve of sample WW10-8 (site C).

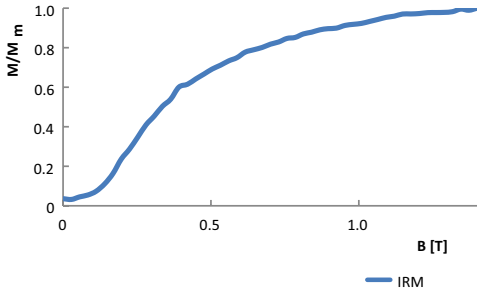

Fig. S6. Normalized IRM curve of sample WW10-8 (site C).

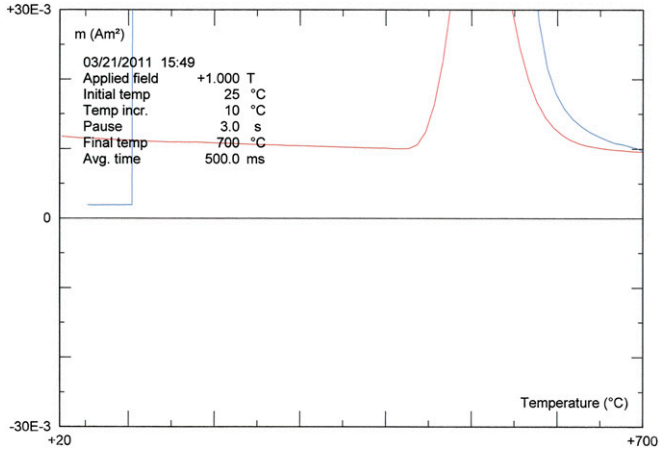

Fig. S7. Single moment-vs.-temperature curve of sample WW10-8 (site C).

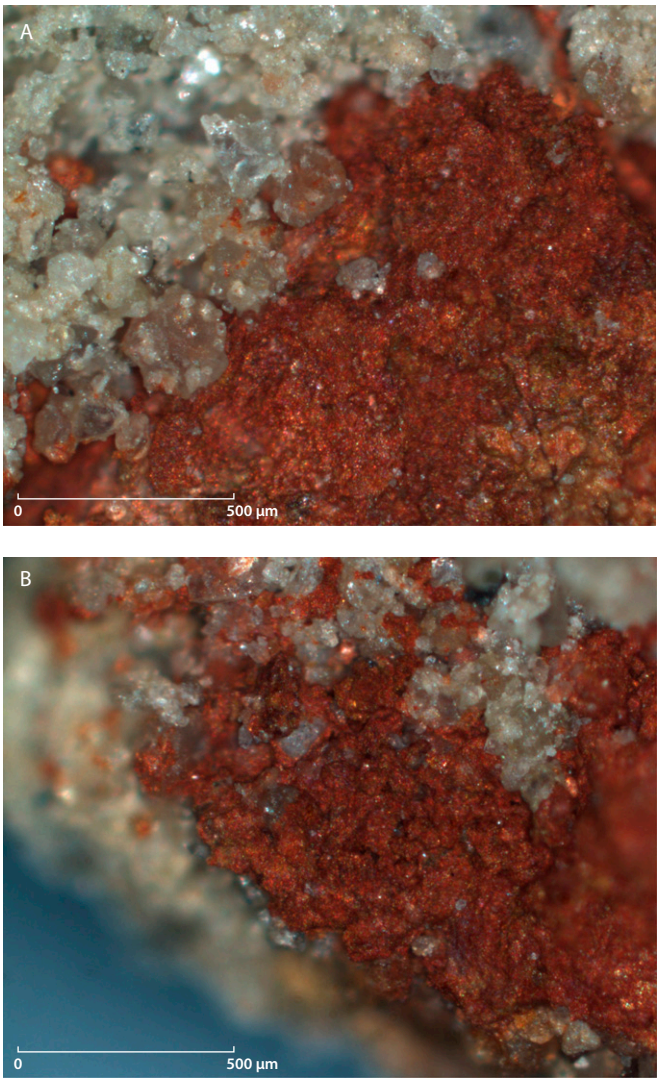

Fig. S8. Close-up views of archeological hematite concentrate Dz20-56 (site C), with its surrounding sandy matrix.

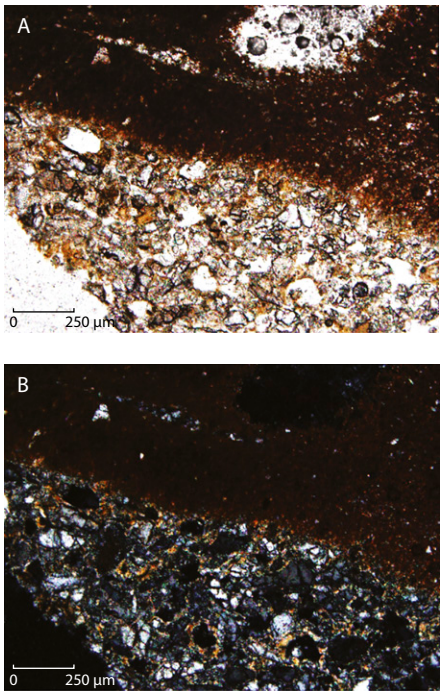

Fig. S9. Thin section of part of sample Bz13-6 (site C), showing a sharp boundary between the sedimentary matrix and the hematite concentrate, as well as a decrease in grain size from the sedimentary matrix (lower left) to the hematite concentrate. (*A*) Plane polarized light. (*B*) Cross polarized light.

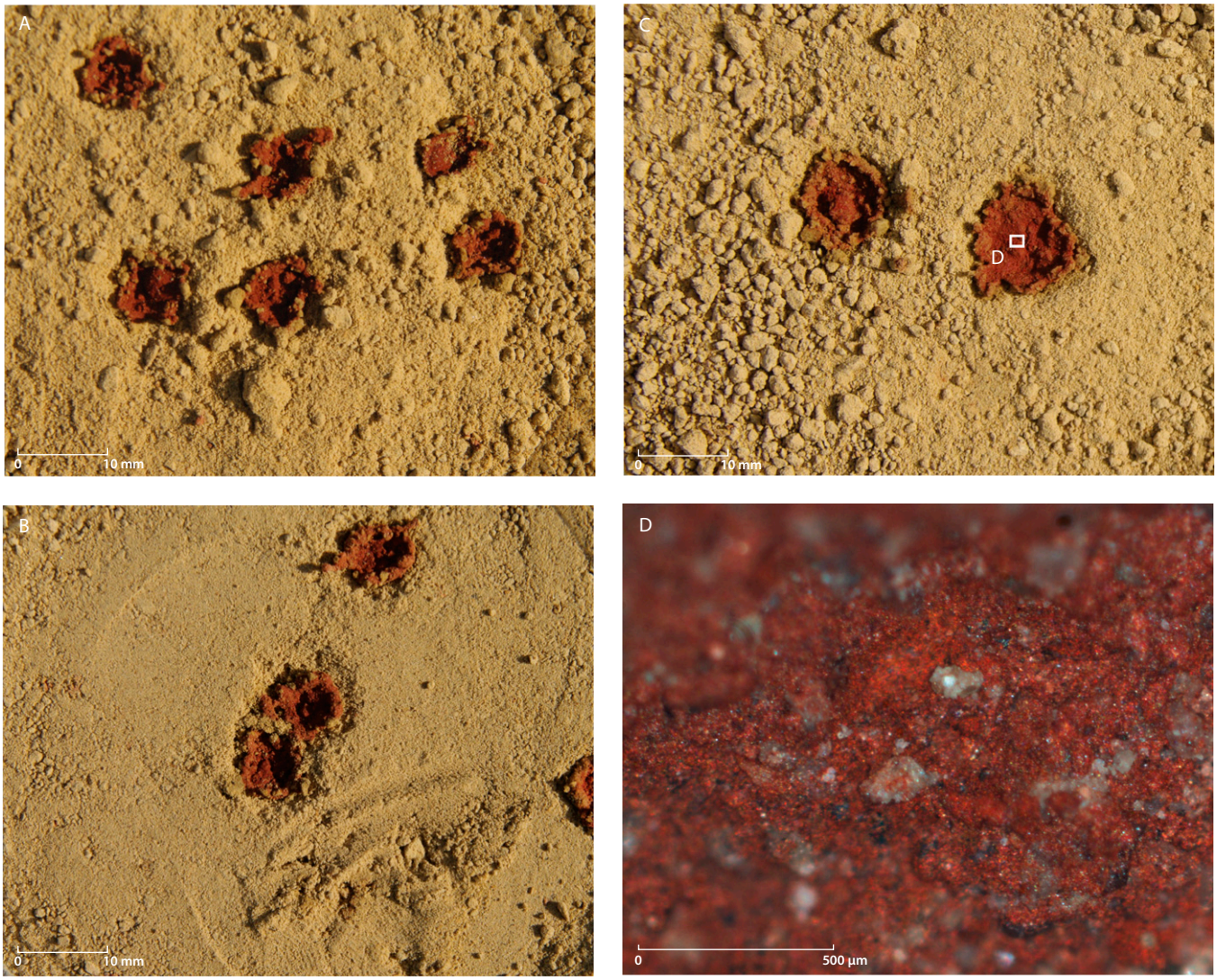

Fig. S10. (*A* and *B*) Experimental hematite dots created on an irregular (*A*) and a "smoothed" (*B*) dry surface (50-cm height, 0.3-cm drops). The concentrates are within small craters produced during impact of the drops on the dry sediment. (*C*) Concentrates created by 0.5-mm drops, launched from a height of 50 cm. (*D*) Close-up view of the inner part of an experimentally produced hematite dot shown in *C* (0.5-cm drops, 50-cm height).

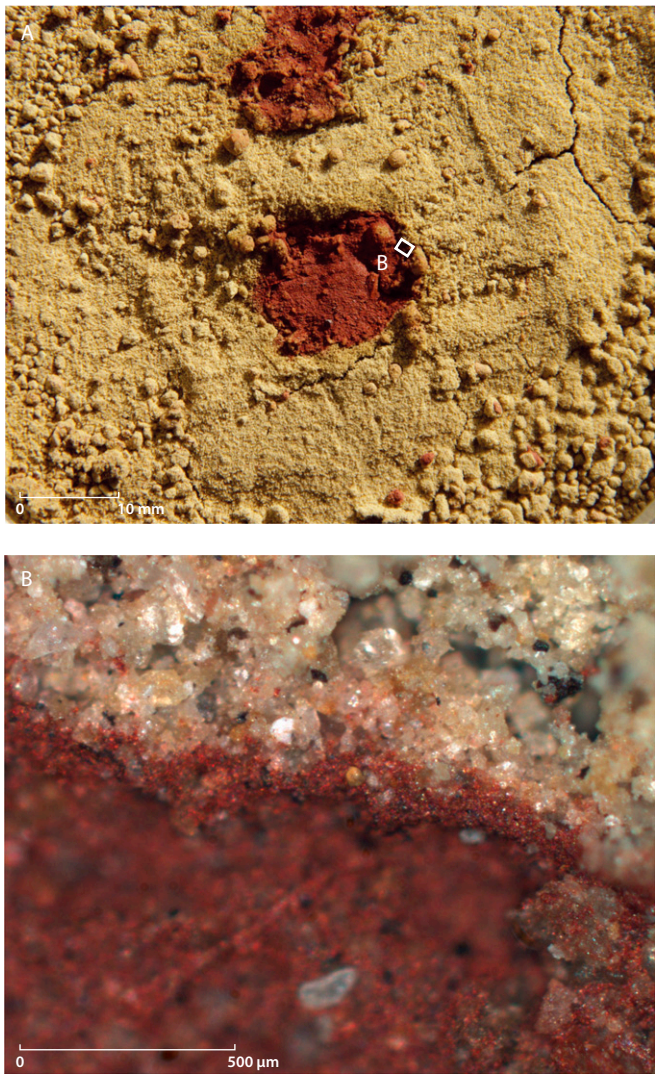

Fig. S11. (*A*) Hematite concentrates created on moist sediment by a 0.5-cm drop launched from a height of 50 cm (see text for explanation). (*B*) Close-up view of the experimental hematite concentrate on "moist" sediment, boundary with sand matrix; see *A* for the position of the close-up.

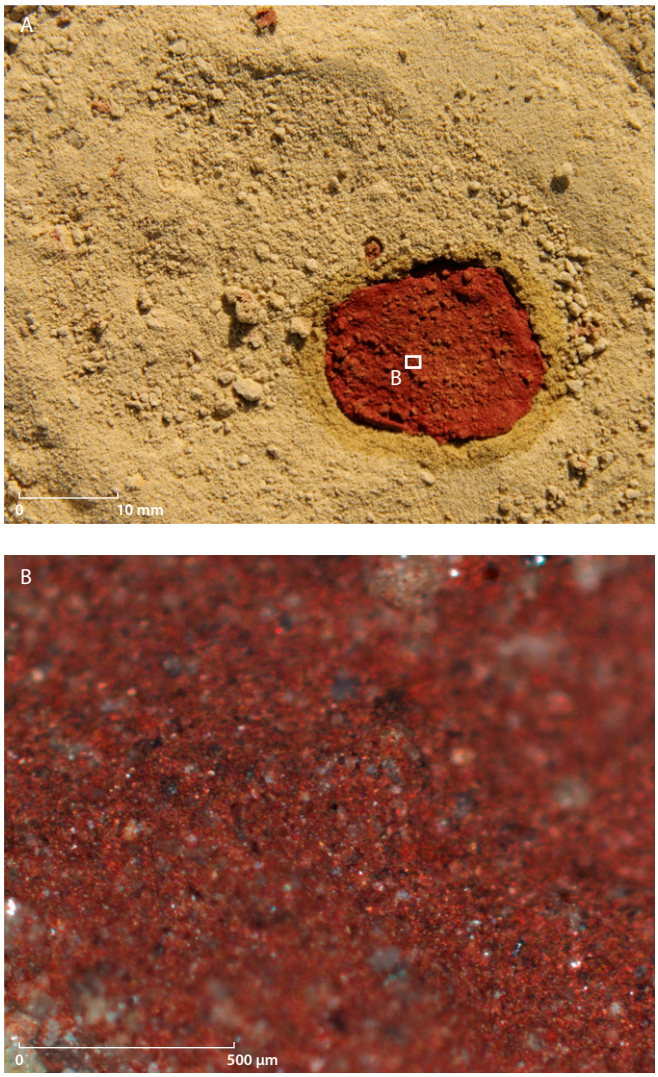

Fig. S12. (*A*) Hematite concentration produced experimentally by pouring 2 mL of the hematite liquid from a test tube onto the dry sediment from a height of 5 cm. (*B*) Close-up view of the experimental hematite concentrate "spill"; see *A* for the position of the close-up.